Published in ***Journal of Porous Materials,*** DOI: 10.1007/s10934-019-00758-2.

# Facile template-free synthesis of hierarchically porous NiO hollow architectures with high-efficiency adsorptive removal of Congo red

Hanmei Hu[a], Chonghai Deng[b*], Mei Sun[a], Kehua Zhang[a], Man Wang[a], Jiayi Xu[b], Huirong Le[c]

[a] Key Laboratory of Functional Molecule Design and Interface Process, Anhui Jianzhu University, Hefei, 230601, China

[b] Department of Chemical and Materials Engineering, Hefei University, Hefei, 230601, China

[c] School of Mechanical Engineering and Built Environment, University of Derby, Derby DE22 3AW, United Kingdom

* Corresponding author. *E-mail address*: chdeng@hfuu.edu.cn; hmhu@ustc.edu.

## Abstract

Hierarchically porous NiO hollow architectures (HPHAs) were synthesized via a one-pot facile chemical bath deposition method and followed by a calcination process. The crystal structure, component and morphology of the products were characterized by various techniques. The results revealed that hierarchical architectures with hollow interior are composed of mesoporous NiO nanoflakes with thickness of about 8 nm. Interestingly, the as-synthesized NiO HPHAs have the unusual three-scaled porous features including a microscale hollow interior and two mesoscale pores which are attributed to the holes on the surface of nanoflakes with an average diameter of about 3.9 nm and the cavities on the wall of microsphere in the range of 20-40 nm in diameter formed by interconnecting nanoflakes. These comprehensive hierarchically porous structures are beneficial for the adsorption performance towards Congo red in water. The absorptive capacity of NiO HPHAs achieved about 1.8 and 4.0 times as

ACCEPTED MANUSCRIPT

high as that of the precursor β-$Ni(OH)_2$ hollow microspheres (HSs) and the commercial activity carbon (AC) under the same conditions. The studies of adsorption kinetics illustrated that the adsorption behavior perfectly obeyed the pseudo-second-order model and the adsorption isotherm fits the Langmuir adsorption assumption well. The maximum adsorption capacities were calculated to be 490.2 $mg \cdot g^{-1}$ according to the Langmuir equation, which is excellent result compared to NiO absorbents. The high-efficiency adsorption capacities for NiO HPHAs are attributed to the large specific surface area, the synergistic effect of micro-mesoporous structure and the electrostatic interaction of NiO with CR molecules. Additionally, NiO HPHAs can be easily renewed and has excellent chemical stability, indicating a great promising absorbent in the application for the removal of diazo organics in wastewater.

***Keywords:*** NiO; hollow structure; pore structure; adsorption; water purification

## 1. Introduction

Hierarchical nanomaterials with hollow interior and mesopores have attracted great interest due to their unique structural features, including low density, high specific surface area, and good surface permeability, which make them promising for applications in many fields such as photonic devices, drug delivery, ionic intercalation, nanocatalysts and nanoreactors [1-3]. The outstanding optical/electrical properties as well as practical industrial applications of such nanomaterials are largely associated with their high surface area and high mass transfer rate due to the presence of pores

ACCEPTED MANUSCRIPT

and cavities. Nickel oxide (NiO), as an important multifunctional transition metal oxide, has represented an impressive kind of materials in ample application fields, such as supercapacitors, battery cathodes, gas sensors, fuel cell electrodes, catalysts, absorbents and so forth [4-8]. In recent decades, numerous efforts have been focused on the development of hollow NiO micro/nanostructures for their enhanced properties and potential applications. Lots of NiO hollow architectures have been created by various template-based methods and typically physicochemical routes [9-30]. Among them, one major strategy for the construction of NiO hollow structures were carried out by the stepwise procedure including the initial preparation of the $Ni^{2+}$-based precursors and followed by the thermal decomposition. For example, NiO hollow spheres were synthesized by using carbon spheres as template for the amperometric glucose biosensor and lithium-ion batteries [11, 12]. Hierarchical NiO hollow spheres toward the superior adsorption or electrochemical activities were fabricated by utilizing polystyrene spheres (PSs) as template [16-18]. Double-shelled NiO hollow nanospheres were constructed by employing metal-organic frameworks (MOFs) as template for the high performance supercapacitors [26]. Elliptical NiO hollow microstructures for high electrochemical energy storage application were prepared by adopting the rape pollen grains as biotemplate [27]. To some extent, the aforementioned various template-based approaches may increase the reaction complexity, suffer from tedious synthetic procedures and thus limit the large-scale applications. In our previous works, a series of hollow architectures such as ZnO, CuO, $Cu_2O$ and CuS have been constructed by the “gas-bubble” template technology

ACCEPTED MANUSCRIPT

[31-35]. No doubt that there is the obvious advantage of avoiding the template removal step in the hollow structure synthesis by using "gas-bubble" as soft template. However, except that Zhu and Kuang fabricated successfully the hollow NiO microspheres through the hydrothermal process [28, 29], there are few publications on the preparation of hollow NiO structures based on the "gas-bubbles" template in the reported references. Due to the hydrothermal process usually suffers from disadvantages related to high-cost and time-consuming, thus it is highly desirable to develop a simple synthetic process that can construct the NiO hollow architectures under the mild conditions for their promising applications.

Congo red (CR), as a typical anionic diazo dye with structural stability, is very difficult to biodegrade and even photodegrade in the practical application. Nevertheless, the adsorption technique has been demonstrated to be a remarkable approach to the removal of CR dye, owing to its high efficiency, simplicity of design, and ease of operation [36-39]. Even though there are a few disadvantages such as low selectivity, slow adsorption rate and low adsorption capacity of absorbents in the industrial application, it is regarded as a good choice to treat wastewaters containing such diazo dyestuffs. Recently, thanks to the positive charged surface and chemical stability of NiO nanocrystal, the feasibility of NiO nanomaterials for the high efficiency adsorptive removal of diazo dye CR in water treatment have emerged in the reported literatures [19, 37, 38].

Herein, hierarchically porous NiO hollow architectures (HPHAs) with the three-scaled porous structure has been fabricated by the calcination of the precursor of

ACCEPTED MANUSCRIPT

flower-like β-$Ni(OH)_2$ hollow spheres (HSs), which were synthesized by a facile chemical bath deposition (CBD) process in the absence of hard templates. The as-synthesized HPHAs with hollow interior are composed of thin NiO porous nanoflakes, which were cross-connected with each other to generate cavities on the wall of sphere. An Ostwald ripening mechanism using $CO_2$ bubbles as template is proposed to explain the formation of the hollow structures. Own to the high surface area, the specific hierarchical porous features and the electrostatic attraction, the use of NiO HPHAs as adsorbent for the removal of CR in wastewater has also been investigated thoroughly.

## 2. Experimental procedure

### 2.1. Sample preparation

All analytically pure chemicals such as nickel chloride hexahydrate ($NiCl_2 \cdot 6H_2O$), aqueous ammonia ($NH_3 \cdot H_2O$, w/w 25~28%) and urea ($H_2NCONH_2$) were purchased from Sinopharm Chemical Reagent Co. Ltd (Shanghai, China) and used as received without further purification. Deionized (DI) water was used to prepare the reaction solution and adsorption experiments.

At first, hierarchically-structured β-$Ni(OH)_2$ hollow spheres (HSs) were synthesized by a facile one-pot chemical bath deposition (CBD) method in the absence of any surfactant and template. In a typical experimental procedure, 1 mmol $NiCl_2 \cdot 6H_2O$, 4 mL $NH_3 \cdot H_2O$ and 2 mmol urea were dissolved in 60 mL DI water under stirring to form a homogeneous solution. The beaker containing the mixture was covered with a piece of polyethylene (PE) film, and then transferred into the water bathing room at

ACCEPTED MANUSCRIPT

the temperature 90 ºC for 4 h under a static condition. After being cooled naturally to room temperature, the sediment was filtered out, washed with DI water and ethanol, and dried at 60 ºC for 8 h in air. Subsequently, the as-prepared β-$Ni(OH)_2$ precursor was annealed at 400 ºC for 2 h with a heating ramp rate of 2 ºC/min under air atmosphere, then the hierarchically porous NiO hollow architectures (HPHAs) were finally obtained. For ease of understanding, the facile template-free CBD and calcination synthesis process for NiO HPHAs is schematically illustrated in **Fig. 1.**

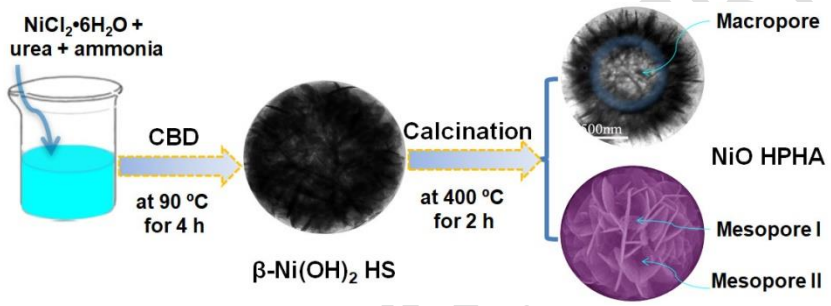


**Fig.1.** Diagram of synthesis of hierarchical β-$Ni(OH)_2$ HSs and NiO HPHAs.

## 2.2. Characterization

The phase purity of the as-synthesized products was examined by X-ray diffraction (XRD) using a Bruker D8-advance X-ray diffractometer equipped with Cu Kα radiation (λ = 1.5406 Å). Field-emission scanning electron microscope (FESEM) images of the sample were taken on a JEOL JSM-6700F field-emission microscope with a voltage of 15kV. The transmission electron microscope (TEM) images of the samples were performed on a JEOL-2010 transmission electron microscope with an accelerating voltage of 200 kV. The optical properties of the CuS suspension were ascertained using an UV-vis Spectrophotometer (UV-5500PC). The BET surface areas were analyzed by nitrogen ($N_2$) adsorption with a Tristar II 3020 M automatic surface

ACCEPTED MANUSCRIPT

area and pore analyzer. All the samples were degassed at 200℃ for 2 h prior to the $N_2$ adsorption measurements.

### 2.3. Absorption activity measurements

The evaluation of the adsorption activity of the as-prepared samples for the removal of diazo dye solution was studied in a batch adsorption experiment performed in a dark thermostatic oscillator at 30 ºC. In a typical kinetic test, adsorption experiments for Congo Red (CR) in water over the samples were performed as follows: 10 mg of the samples were added into 50 mL of CR solution (20~120 $mg \cdot L^{-1}$) at pH = 7.0. At different adsorption time, the suspension was separated by centrifugation, and analytical samples were taken from the top clear liquid. The CR concentration was determined by measuring the solution characteristic absorption at 497 nm using UV-vis Spectrophotometer (UV-5500PC, Shanghai). The amount of CR adsorbed per unit mass of the adsorbent was calculated by the following equation (1). The procedures for equilibrium studies were quite similar to the kinetic experiments. The as-synthesized samples (10 mg) were placed into conical glass flasks containing 50 mL of CR solutions with varied concentrations (20~120 $mg \cdot L^{-1}$). The conical flasks were shaken for 12 h in a thermostatic oscillator to achieve equilibrium. The CR adsorption amount at equilibrium, $q_{eq}$ ($mg \cdot g^{-1}$), was calculated by equation (2) [36, 37].

$$q_t = (C_0 - C_t)V/W \quad (1)$$

$$q_{eq} = (C_0 - C_{eq})V/W \quad (2)$$

Where $q_t$ and $q_{eq}$ ($mg \cdot g^{-1}$) are the amount adsorbed per gram of adsorbent at

ACCEPTED MANUSCRIPT

adsorption time (t, min) and at equilibrium, $C_0$, $C_t$ and $C_{eq}$ ($mg \cdot L^{-1}$) are CR aqueous concentrations initially, at adsorption time, and at equilibrium, while $V$ (L), and $W$ (g) are the volume of CR solution, and the adsorbent mass, respectively.

## 3. Results and discussion

### 3.1. Morphologies and chemical composition analysis

**Fig. 2** displays the typical X-ray diffraction patterns of the as-resulting samples prepared by the single-pot BCD process and subsequent heat treatment. As given in **Fig. 2a**, the diffraction peaks are in good agreement with the standard data from JCPDS card no. 14-0117, and are identified to hexagonal phase β-$Ni(OH)_2$ with the $P6_3/m$ space group and a primitive hexagonal unit cell with a = b = 3.126 Å and c = 4.605 Å. No other peak is observed belonging to the impurities, suggesting the high purity of the as-synthesized β-$Ni(OH)_2$. As illustrated in **Fig. 2b**, the diffraction peaks at 37.24°, 43.27° and 62.87° can be assigned to (111), (200) and (220) planes of the face-centered cubic (FCC) NiO with the lattice constant of a = 4.188 Å (JCPDS 47-1049). The strong and sharp diffraction peaks indicate that the as-prepared sample have the high crystallinity. No peaks due to β-$Ni(OH)_2$ are observed, indicating that β-$Ni(OH)_2$ is completely converted to NiO after calcination treatment. In addition, the relatively broader diffraction peaks suggest that the smaller crystallite size for NiO grains formed at the stage of the thermal decomposition.

ACCEPTED MANUSCRIPT

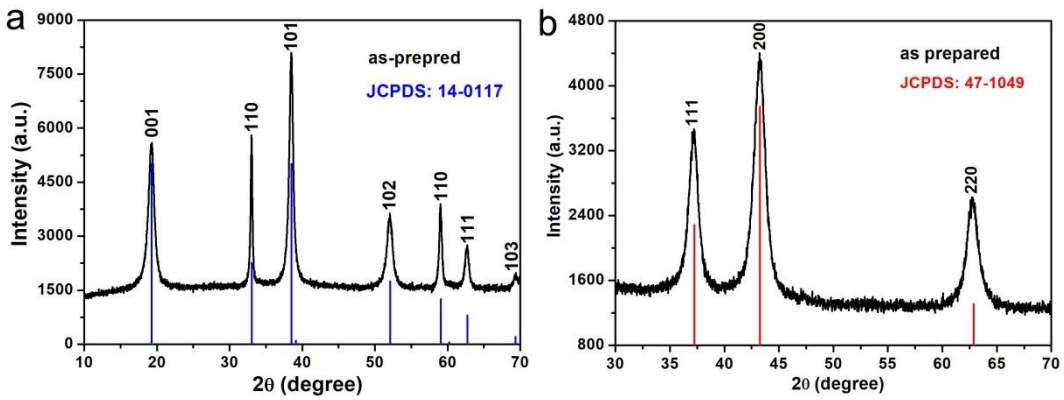


**Fig.2.** XRD patterns of (a) as-prepared precursors and (b) the annealed products.

The morphology and microstructure of the as-synthesized products were investigated by FESEM and TEM. As displayed in **Fig. 3a**, the large-scaled mono-dispersed $Ni(OH)_2$ particles have the quasi-spherical structures with the diameter in the micron range. A typical elegant flower-like sphere is inserted in Fig.3a, from which it can be found that the ultrathin twisted nanosheets intercalate with each other to form the shell with the ragged surface. **Fig. 3b** is a representative TEM picture for $Ni(OH)_2$ flower-like spheres. The obvious contrasts between the dark edge and pale center are the evidence of the hollow nature. Besides, it is clear that the shells of the hollow spheres are composed of intercrossed nanosheets, being in agreement with FESEM results. From the magnification TEM image (insert in **Fig. 3b**), it can be further determined that the nanosheets are very thin by the similar contrast between the nanosheet margin and the background.

ACCEPTED MANUSCRIPT

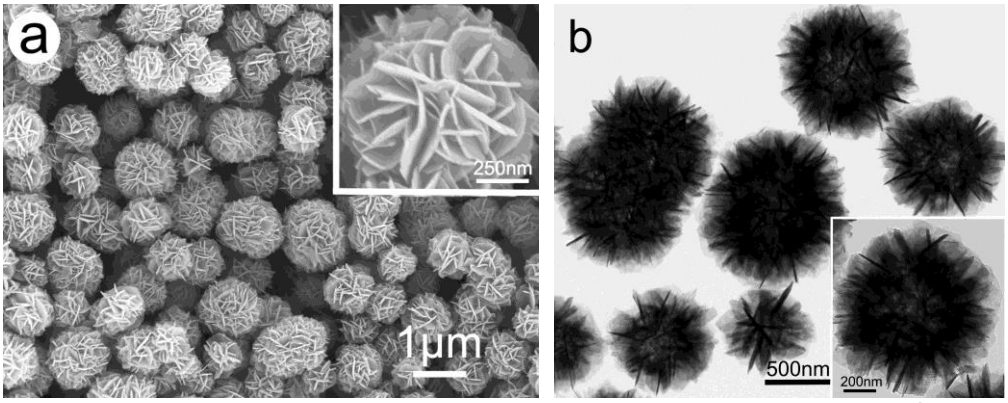


**Fig. 3.** FESEM and TEM images of as-prepared $Ni(OH)_2$ by CBD method.

The flower-like $Ni(OH)_2$ hollow spheres (HSs) were transferred to monolithic NiO after the annealing process, which maintained the precursor original morphology. As shown in **Fig. 4a**, FESEM overview observation reveals that the overall morphology of NiO particles displays the elegant hydrangea-like sphere in shape with the outer-diameters in the range of 0.8-1.2 μm. The walls of spheres are constituted with the ultrathin and porous NiO nanoflakes confirming by the high magnification SEM image (**Fig. 4b)**. There are a large amount of holes scattered on the surface of nanoflakes of which the average thicknesses are about 8 nm. The twisted nanoflakes interconnect with each other to form the unique crateriform-like cavities with varying dimensions of 20~40nm on the wall of sphere. A representative TEM picture is given in **Fig. 4c**. It can be observed that NiO sphere possesses a huge hollow interior, the wall of which are comprised of the interlaced nanoflakes with porous channels and cavities, being in agreement with FESEM results. The high-resolution TEM (HRTEM) image is shown in **Fig. 4d**. The well-resolved lattice fringes in HRTEM image correspond to an interplanar spacing of 0.241 nm, consistent with the (111) planes of FCC NiO. In addition, as given in **Fig. 4e**, the corresponding selected area electronic

ACCEPTED MANUSCRIPT

diffraction (SAED) pattern is characterized as the electron diffraction rings, which is further indexed with the cubic NiO phase (JCPDS 47-1049), indicating the polycrystalline features of the as-prepared hierarchically porous NiO hollow architectures (HPHAs).

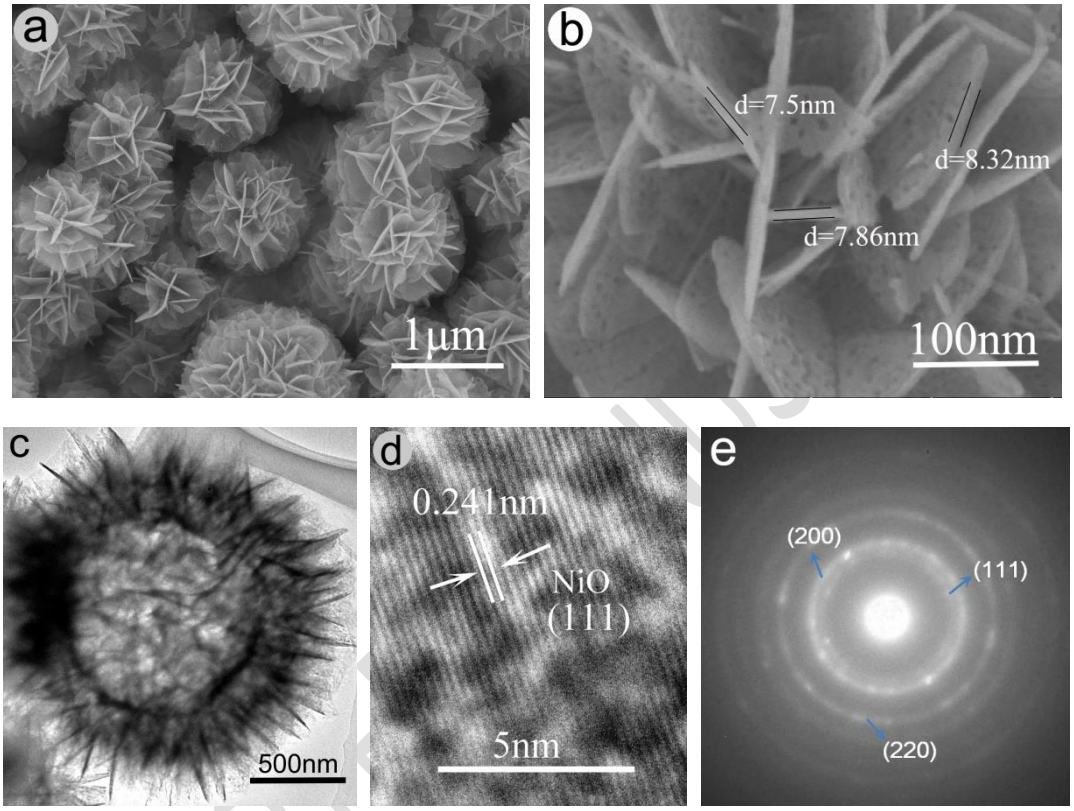


**Fig.4.** FESEM (a and b), TEM (c) and HRTEM (d) images, and SAED pattern (e) of as-prepared NiO HPHAs.

3.2. Plausible growth mechanism

In the reaction system, ammonia aqueous ($NH_3 \cdot H_2O$) and urea play the important roles for the formation of flower-like $Ni(OH)_2$ HSs in the BCD process. $NH_3 \cdot H_2O$ may not only act as an organic base but also as a good complexing reagent with metal ions due to a lone pair of electrons on the nitrogen atom. Meanwhile, urea can decompose at the reaction temperature to supply microbubbles in the nucleation

condition acting as soft templates for the formation of hollow structures. While $NH_3 \cdot H_2O$ was introduced into the $Ni^{2+}$ ions solution, the dissociated $NH_3$ and $H_2O$ molecules [(Eq.3)] coordinate promptly with $Ni^{2+}$ ions to form $[Ni(H_2O)_{6-x}(NH_3)_x]^{2+}$ complexes [(Eq.4)] [28, 40]. The Eq.4 is a reversible reaction, which can slowly release the free configurational ions in solution and control the crystal nuclei formation and growth rate. While under the condition of water-bathing heating at the temperature of 80 °C, urea can hydrolyze to produce carbon dioxide ($CO_2$) and $NH_3$ into the aqueous solution [(Eq.5)] [31], which can not only drive $NH_3 \cdot H_2O$ ionization to generate $OH^-$ ions [(Eq.3)] but also generate the numerous gas/liquid interface of microbubbles ($CO_2$) in the micro environment. Then newly-dissociated $Ni^{2+}$ and $OH^-$ ions react immediately to generate the $Ni(OH)_2$ nuclei [(Eq.6)]. Those newly-formed $Ni(OH)_2$ nuclei are apt to self-aggregate around the microbubbles driven by the incentive for the decreasing of interfacial energy. Due to the layered structure of the $CdI_2$ type with weak interaction between layers *via* van der Waals forces [41], the brucite $Ni(OH)_2$ crystals are prone to forming two-dimensional (2D) nanostructures. Along with $Ni(OH)_2$ nuclei growing into nanocrystals, the interconnected nanosheets self-assembled to form the hollow flower-like microspheres. After secondary crystal growing and Ostwald ripening, the hierarchical $Ni(OH)_2$ HSs may be fabricated by the BCD method, where the $CO_2$ microbubbles act as the soft templates. If without urea, the products are of nanosheets rather than flower-like microspheres with hollow interior, which was determined under the hydrothermal conditions [28]. The similar possible schematic diagram of the formation process of hierarchical hollow structures

ACCEPTED MANUSCRIPT

was illustrated in our previous reports [31, 32]. Finally, NiO HPHAs were obtained by the calcination of the precursor $Ni(OH)_2$ HSs [(Eq.7)]. During the decomposition process, the release of $H_2O$ gases leads to the formation of holes in NiO nanoflakes. Thus the plausible schematic illustration of the formation mechanism of NiO HPHAs was elaborated in detail in **Fig.5**, and all the chemical reactions involving the CBD method and calcination treatment may be expressed as follows [28, 42]:

$$NH_3 + H_2O \leftrightarrow NH_3 \cdot H_2O \leftrightarrow NH_4^+ + OH^- \quad (3)$$

$$Ni^{2+} + xNH_3 + (6\text{-}x)\ H_2O \leftrightarrow [Ni(H_2O)_{6-x}(NH_3)_x]^{2+} \quad (4)$$

$$CO(NH_2)_2 + 2H_2O \rightarrow 2NH_3 \uparrow + CO_2 \uparrow \quad (5)$$

$$Ni^{2+} + 2OH^- \rightarrow Ni(OH)_2 \downarrow \quad (6)$$

$$Ni(OH)_2 \rightarrow NiO + H_2O \quad (7)$$

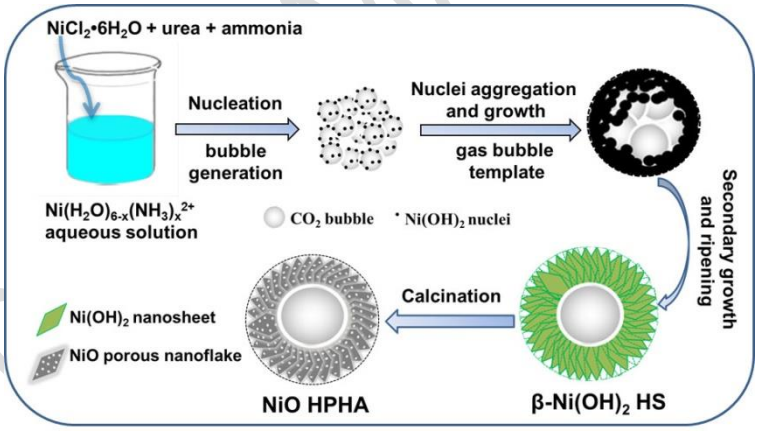


**Fig.5.** Plausible schematic illustration of the formation mechanism of NiO HPHA.

3.3. Specific surface areas and porosity

The specific surface area and the pore size distribution of NiO HPHAs and $Ni(OH)_2$ HSs were studied by nitrogen adsorption. The BET specific surface area of NiO was calculated to be 117.0 $m^2/g$, which is very high for transition metal oxide materials with sizes in the micron range, and higher than that of $Ni(OH)_2$ HSs (87.4 $m^2/g$). As

given in **Fig. 6a**, the nitrogen sorption isotherms of the precursor and NiO sample display type IV isotherms with $H_3$-type loop hysteresis, indicating the existence of mesopores in the samples [43]. From the corresponding pore size distribution curve (**Fig. 6b**), the typical bimodal pore structures were observed, in which the pore sizes were calculated to be 3.82 and 27.96 nm in diameter, respectively. As depicted in SEM image (inset in **Fig. 6b**), the smaller mesopore I should be attributed to the tiny porous channels on the surface of nanoflakes whereas the larger mesopore II should be attributed to the cavities on the wall formed by interconnecting nanoflakes. Taking into account the micropore of hollow interior, the as-prepared NiO HPHAs with the unusual three-ordered hierarchically porous structures have been constructed successfully. It is expectable that the considerably high surface area and the special hierarchical pore structure make it a promising candidate as an absorbent for the removal of dye pollution in wastewater purification.

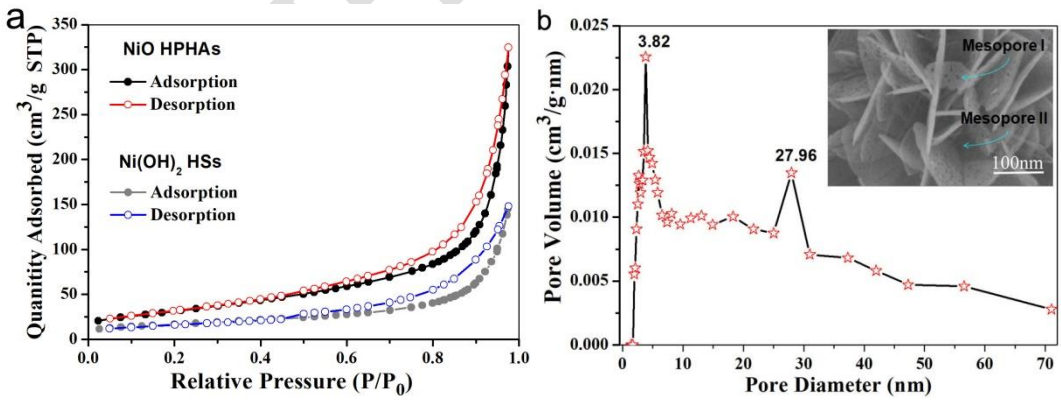


**Fig.6.** Nitrogen adsorption/desorption isotherm (a) and pore size distribution curve (b) of as-prepared NiO HPHAs.

## 3.4. Comparison of adsorption capacity

The adsorption experiments of NiO HPHAs in aqueous CR solution were carried out

by given contact time studies for the different CR concentration at 30 ºC (pH=7.0). Besides, for comparison of adsorption preformation, the precursor $Ni(OH)_2$ HSs and the commercial active carbon (AC) were chosen as contrast absorbents under the same test condition, in which AC is of importance to the adsorption of dye pollutants in the industrial wastewater purification. **Fig. 7a** shows the evolution in UV-Vis spectra during the absorptive removal of CR with the initial concentration of 20 $mg \cdot L^{-1}$ over NiO HPHAs. Significantly, the main absorption peak for CR molecule locates at 497 nm, which decreases abruptly at the initial 2 min of adsorption time. Moreover, there is no absorption peak in the whole spectrum after 20 min of adsorption, indicating the complete removal of CR in solution. The corresponding photograph of CR at different adsorption time is displayed in the inset of **Fig. 7a**, in which the orange red color of the starting CR solution fades obviously and almost disappears within 20 min of absorption, exhibiting fast and highly efficient absorption of the absorbent. **Fig. 7b** displays the comparison of adsorption capacities of aqueous CR with the starting concentration of 40 $mg \cdot L^{-1}$ in the presence of different absorbents (red line: NiO HPHAs, green line: β-$Ni(OH)_2$ HSs and black line: AC). It can be observed that the adsorption process over NiO HPHAs achieved the equilibrium after about 60 min, whereas the adsorption equilibrium was reached over $Ni(OH)_2$ HSs beyond 240 min of adsorption, and it was not realized over AC even after 360 min of adsorption. The results indicate that NiO HPHAs have the faster adsorption of CR dye than that of the other two absorbents. Furthermore, the adsorption amounts of NiO HPHAs for CR within 60 min are calculated to be 191.7 $mg \cdot g^{-1}$, which is about 1.8

ACCEPTED MANUSCRIPT

and 4.0 times as high as that of $Ni(OH)_2$ HSs (108.0 $mg \cdot g^{-1}$) and AC (48.0 $mg \cdot g^{-1}$) under the same experimental condition, displaying the more efficient adsorption of NiO HPHAs compared with the other two samples.

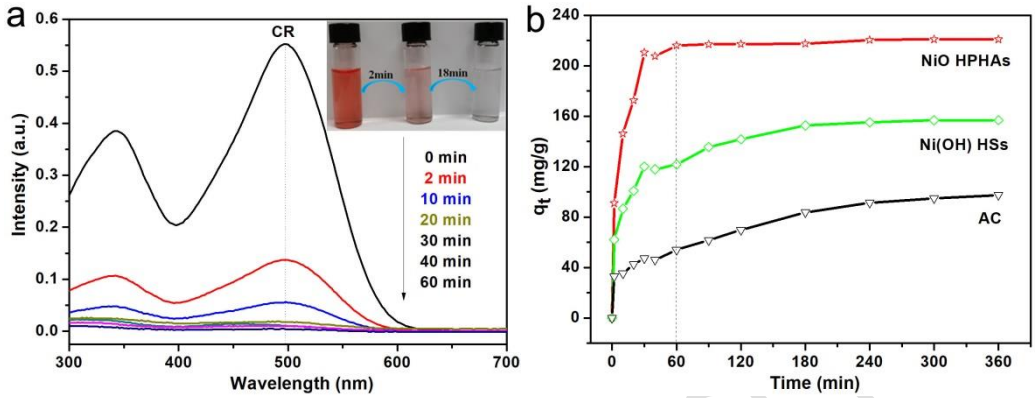


**Fig. 7.** (a) The changes of UV-Vis spectra during the removal of CR over NiO HPHAs and (b) Comparison of adsorption capacities for CR with different absorbents.

3.5 Adsorption kinetics

For the understanding of the sorption mechanism, the adsorption tests at different CR initial concentration (20~80 $mg \cdot L^{-1}$) were performed over NiO HPHAs sample at 30 ºC (pH=7.0). As shown in **Fig. 8a**, the adsorption kinetics at different CR concentrations reveal that the adsorption in all experiments was fast in the initial 30 min, and then the adsorption rates gradually decreased and the adsorption was in equilibrium within 90 min. The adsorption kinetics of CR onto NiO HPHAs was investigated by the pseudo-second-order kinetic model that the equation can be expressed as follows:

$$\frac{t}{q_t} = \frac{1}{k_c q_e^2} + \left(\frac{1}{q_e}\right) t \tag{8}$$

where $k_c$ ($g \cdot mg^{-1} \cdot min^{-1}$) is the rate constant of pseudo-second-order reaction, $q_e$ and $q_t$ ($mg \cdot g^{-1}$) are the adsorption amount of CR onto NiO HPHAs at equilibrium and time t

(min), respectively. The plot of $t/q_t$ against $t$ is shown in **Fig. 8b**. From the slope and intercept of line, the values of $k_c$ ($\times 10^{-4}$ g·mg$^{-1}$·min$^{-1}$) is calculated to be 183.54, 14.51, 7.46 and 5.54 for the starting CR concentrations of 20, 40, 60 and 80 mg·L$^{-1}$, respectively. Furthermore, all the values of corresponding correlation coefficient ($R^2$) are very close to 1, indicating that the adsorption of CR onto NiO HPHAs obeys perfectly the pseudo-second-order model reaction.

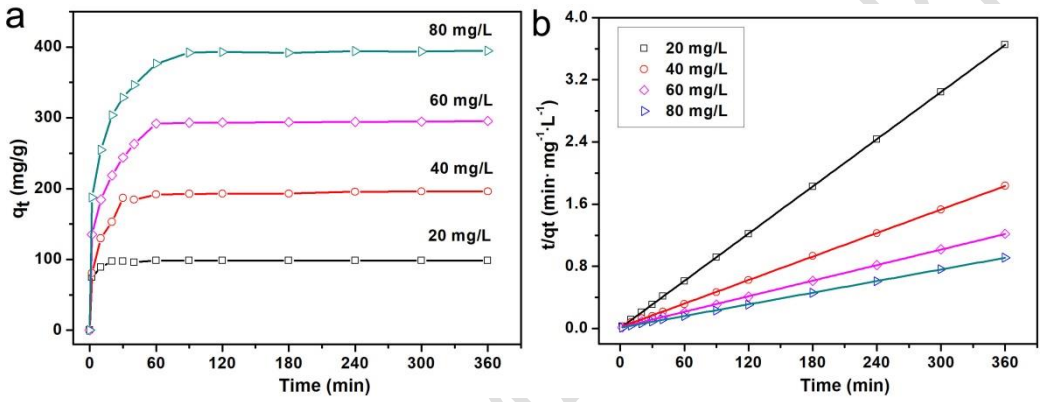


**Fig. 8.** (a) Changes of adsorption capacities for CR over NiO HPHAs at different initial CR concentrations and (b) pseudo-second-order kinetics for CR adsorption with NiO HPHAs.

3.6 Adsorption isotherms

Adsorption isotherms were used to study the adsorption capacity of the sample at different equilibrium CR concentrations (20~120 mg·L$^{-1}$). The Langmuir equation presumes that there is no interaction among the adsorbate molecules and all the adsorption sites are uniform where the sorption is only localized in a monolayer. If a dye molecule occupies an active adsorptive site, no further adsorption can take place at the site. The Langmuir equation is expressed as follows:

$$q_e = \frac{q_{max} K_L c_e}{1 + K_L c_e} \quad (9)$$

where $q_e$ (mg·g$^{-1}$) is the equilibrium adsorption amount of CR on per unit mass of

adsorbent, $c_e$ (mg·L$^{-1}$) is the equilibrium concentration of CR, $q_{max}$ (mg·g$^{-1}$) is the theoretical maximum adsorption capacity of the adsorbent corresponding to complete monolayer coverage on the surface, and $K_L$ (L·mg$^{-1}$) is the Langmuir adsorption constant and related to the free energy of adsorption. The Langmuir equation can be rearranged to a linear form, and the values of $q_{max}$ and $K_L$ can be calculated from the slope and intercept of the linear plot of $c_e/q_e$ against $c_e$:

$$\frac{c_e}{q_e} = \frac{1}{q_{max}K_L} + \frac{1}{q_{max}}c_e \quad (10)$$

As presented in **Fig. 9**a, the adsorption isotherm curve of CR onto NiO HPHAs fits the Langmuir adsorption assumption very well. The corresponding plot of $C_e/q_e$~$C_e$ based on the Langmuir isotherm is shown in **Fig. 9b**. The linear correlation coefficient ($R^2$) is 0.9998. The conformation of the experimental data to the Langmuir isotherm model demonstrats the formation of monolayer coverage of CR molecule on the surface of NiO nanoflakes, indicating the homogeneous feature of the surface of NiO absorbent and the equal adsorption activation energy for each dye molecule/adsorbent adsorption. In addition, the maximum adsorption capacity is calculated to be 490.2 mg·g$^{-1}$ according to the Langmuir equation, which is in fact larger than most of the reported NiO materials summarized in **Table 1**. Based on the above analysis, the as-prepared NiO HPHAs is a potentially more efficient adsorbent for diazo organic dyes compared with NiO other materials.

ACCEPTED MANUSCRIPT

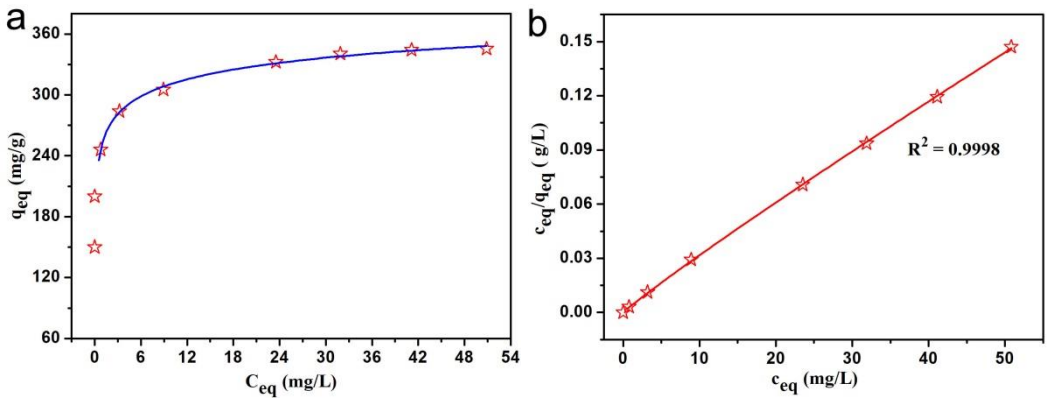


**Fig. 9.** (a) Langmuir adsorption isotherm curve and (b) the plot of $C_e/q_e$~$C_e$ for the adsorption of CR onto NiO HPHAs.

**Table 1.** Adsorption capacities of CR onto the reported NiO materials.

| NiO Adsorbents | Adsorption capacities ($Q_{max}$, mg/g) | References |
|---|---|---|
| NiO HPHAs | 490.2 | This work |
| NiO (111) nanosheets | 36.1 | [44] |
| NiO nanosheets (10nm thick) | 151.7 | [45] |
| NiO nanosheets | 168 | [46] |
| NiO porous nanobisciuts | 193.2 | [39] |
| NiO porous architectures | 223.8 | [47] |
| NiO roselike microspheres | 342.8 | [38] |
| NiO microspheres | 397.0 | [37] |
| NiO hollow nanospheres | 526.3 | [18] |
| NiO flower-like microspheres | 534.8 | [48] |
| NiO/grapheme nanosheets | 123.9 | [49] |
| ZnO/NiO hollow microspheres | 518.0 | [37] |

ACCEPTED MANUSCRIPT

3.7 Regeneration behaviors

The regeneration capability of the adsorbent is very important for the practical application in wastewater purification. The renewed NiO HPHAs were yielded via the thermal desorption method to remove CR molecule from the surface of NiO. Herein, the reused desorption experiment of CR from NiO adsorbent was operated by the calcination at 500°C for 1 h. The measurement conditions for the cycling experiments are consistent with Fig. 7b. The experimental results of cycling test are shown in Fig. 10. After five cycling runs, the decolorisation rate of CR still maintains at above 90%, showing the far higher adsorption capacity than AC (48.0 $mg \cdot g^{-1}$). Furthermore, SEM image and XRD pattern (inset) of the $5^{th}$ run recovered sample is given in Fig.10b. Besides a few scattered nanosheets (indicated by the blue arrows), the pure phase NiO particles present are still intact spherical structures aggregated by nanosheets, suggesting a good chemical stability. Thus one can conclude that NiO HPHAs would be an attractive candidate as an adsorbent for practical industrial wastewater treatment.

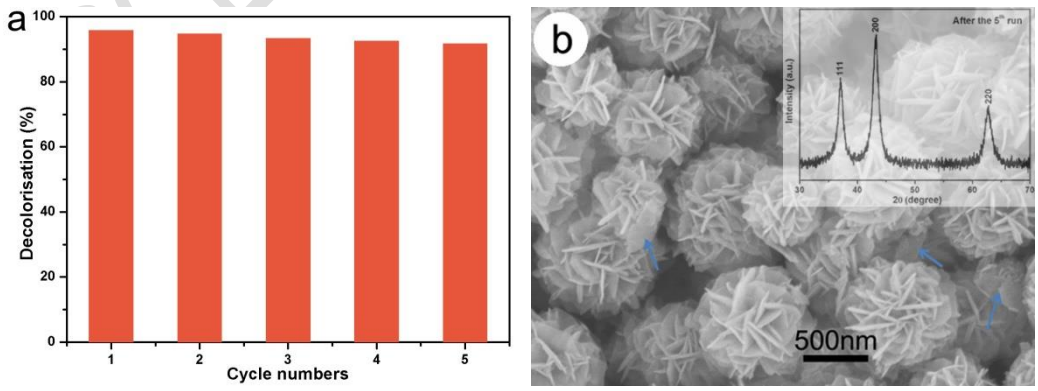


**Fig. 10.** (a) Recycling tests for the decolorisation of CR solution and (b) SEM image of NiO sample after 5 cycling runs (inset: XRD pattern)

ACCEPTED MANUSCRIPT

### 3.8 Adsorption mechanism

As known, the adsorption activities of adsorbents are mainly attributed to their specific surface area and the interaction between groups of adsorbent and adsorbate. In fact, electrostatic attraction between the surface of adsorbent and adsorbate molecule is an important factor influencing the adsorption performance of adsorbent materials [37, 50, 51]. In this system, NiO HPHAs possesses the large specific surface area and hierarchically porous structure, which can provide more available active adsorption sites and efficient transport pathways, resulting in the enhancement of adsorption property. Additionally, owing to the unique three-scaled hierarchically porous structures of NiO HPHAs, CR molecules may enter into the inner space through the holes on the surface of NiO nanoflakes and can remain in the inside of hollow architectures due to the effect of repulsive force. Furthermore, due to the isoelectric point of NiO is about 11.3 and the zeta potential of NiO is positive, thereby the electrostatic interaction between NiO HPHAs and CR molecules should be an reasonably favorable factor for the high adsorption performance of CR onto NiO HPHAs, because the zeta potential value of CR sample is -41.3 mV indicating the negative charge surface in the neutral water environment [37]. In summary, NiO HPHAs demonstrated excellent adsorption capacity towards CR molecules which may be contributed to three factors: the large specific surface area, the synergistic effect of porous structure and the electrostatic attraction of NiO HPHAs with CR.

## 4. Conclusions

ACCEPTED MANUSCRIPT

Hierarchically porous NiO hollow architectures were fabricated by a simple CBD method in the absence of surfactant and followed by calcination. The hollow architectures are composed of the porous NiO nanoflakes with about 8 nm in thickness as well as lots of cavities on the wall formed by nanoflakes interconnected with each other. The plausible crystal growth mechanism of NiO HPHAs was also presented. When employed as adsorbent, the as-prepared NiO HPHAs revealed a high efficient adsorption performance which contributed to the large specific surface area, the synergistic effect of porous structure and the electrostatic attraction of NiO with CR molecules. The adsorption kinetics for CR molecules onto NiO HPHAs followed the pseudo-second-order model and the equilibrium data fitted the Langmuir model well. In view of the hierarchically porous feature and chemical stability, the as-synthesized NiO HPHAs could be a potential alternative for the removal of diazo organics in water as well as a catalyst support for the application in photocatalytic technology.

ACCEPTED MANUSCRIPT

## Acknowledgements

This work was supported by the Natural Science Foundation of Anhui Province (KJ2018A0511, 1808085MB40), and the Key Projects of Support Program for Outstanding Young Talents of Anhui Province (gxyqZD2016151), and the Program of Study Abroad for Excellent Young Scholar of Anhui Province (gxfxZD2016221).

## References

[1] Lou, X.W.; Li, C.M.; Archer, L.A. Designed synthesis of coaxial $SnO_2$@carbon hollow nanospheres for highly reversible lithium storage. *Advanced Materials* **2009**, *21*, 2536-2539.

[2] Lai, X.; Halpert, J.E.; Wang, D. Recent advances in micro-/nano-structured hollow spheres for

energy applications: From simple to complex systems. *Energy and Environmental Science* **2012**, *5*, 5604-5618.

[3] Shen, L.; Yu, L.; Yu, X.Y.; Zhang, X.; Lou, X.W.D. Self-templated formation of uniform $NiCo_2O_4$ hollow spheres with complex interior structures for lithium-Ion batteries and supercapacitors. *Angewandte Chemie - International Edition* **2015**, *54*, 1868-1872.

[4] Xu, X.; Liang, J.; Zhou, H.; Ding, S.; Yu, D. The preparation of hierarchical tubular structures comprised of NiO nanosheets with enhanced supercapacitive performance. *RSC Adv.* **2014**, *4*, 3181-3187.

[5] Wang, X.; Qiao, L.; Sun, X.; Li, X.; Hu, D.; Zhang, Q.; He, D. Mesoporous NiO nanosheet networks as high performance anodes for Li ion batteries. *Journal of Materials Chemistry A* **2013**, *1*, 4173.

[6] Zhang, J.; Zeng, D.; Zhu, Q.; Wu, J.; Huang, Q.; Xie, C. Effect of Nickel Vacancies on the Room-Temperature $NO_2$ Sensing Properties of Mesoporous NiO Nanosheets. *The Journal of Physical Chemistry C* **2016**, *120*, 3936-3945.

[7] Li, Z.; Wei, L.; Liu, Y.; Su, Y.; Dong, X.; Zhang, Y. Facile synthesis of single-crystalline mesoporous NiO nanosheets as high-performance anode materials for Li-ion batteries. *Journal of Materials Science: Materials in Electronics* **2017**, *28*, 13853-13860.

[8] Xu, X.; Li, L.; Yu, F.; Peng, H.; Fang, X.; Wang, X. Mesoporous high surface area NiO synthesized with soft templates: Remarkable for catalytic $CH_4$ deep oxidation. *Molecular Catalysis* **2017**, *441*, 81-91.

[9] Wang, Y.; Zhu, Q.; Zhang, H. Fabrication of $\beta$-$Ni(OH)_2$ and NiO hollow spheres by a facile template-free process. *Chemical Communications* **2005**, 5231-5233.

[10] Liu, J.; Du, S.; Wei, L.; Liu, H.; Tian, Y. Chen, Y. Template-free synthesis of NiO hollow microspheres covered with nanoflakes. *Materials Letters* **2006**, *60*, 3601-3604.

[11] Li, C.; Liu, Y.; Li, L.; Du, Z.; Xu, S.; Zhang, M.; Yin, X.; Wang, T. A novel amperometric biosensor based on NiO hollow nanospheres for biosensing glucose. *Talanta* **2008**, *77*, 455-459.

[12] Cui, Z.; Yin, H.; Nie, Q.; Qin, D.; Wu, W.; He, X. Hierarchical flower-like NiO hollow microspheres for non-enzymatic glucose sensors. *Journal of Electroanalytical Chemistry* **2015**, *757*, 51-57.

[13] Huang, X.H.; Tu, J.P.; Zhang, C.Q.; Zhou, F. Hollow microspheres of NiO as anode materials for lithium-ion batteries. *Electrochimica Acta* **2010**, *55*, 8981-8985.

[14] Cao, C.-Y.; Guo, W.; Cui, Z.-M.; Song, W.-G.; Cai, W. Microwave-assisted gas/liquid interfacial synthesis of flowerlike NiO hollow nanosphere precursors and their application as supercapacitor

ACCEPTED MANUSCRIPT

electrodes. *Journal of Materials Chemistry* **2011**, *21*, 3204-3209.

[15] Cho, N.G.; Hwang, I.-S.; Kim, H.-G.; Lee, J.-H.; Kim, I.-D. Gas sensing properties of p-type hollow NiO hemispheres prepared by polymeric colloidal templating method. *Sensors and Actuators B: Chemical* **2011**, *155*, 366-371.

[16] Ding, S.; Zhu, T.; Chen, J.S.; Wang, Z.; Yuan, C.; Lou, X.W. Controlled synthesis of hierarchical NiO nanosheet hollow spheres with enhanced supercapacitive performance. *Journal of Materials Chemistry* **2011**, *21*, 6602-6606.

[17] Yu, W.; Jiang, X.; Ding, S.; Li, B.Q. Preparation and electrochemical characteristics of porous hollow spheres of NiO nanosheets as electrodes of supercapacitors. *Journal of Power Sources* **2014**, *256*, 440-448.

[18] Zhang, P.; Ma, X.; Guo, Y.; Cheng, Q.; Yang, L. Size-controlled synthesis of hierarchical NiO hollow microspheres and the adsorption for Congo red in water. *Chemical Engineering Journal* **2012**, *189-190*, 188-195.

[19] Zhao, J.; Wu, L.; Zou, K. Fabrication of hollow mesoporous NiO hexagonal microspheres via hydrothermal process in ionic liquid. *Materials Research Bulletin* **2011**, *46*, 2427-2432.

[20] Al-Hazmi, F.; Al-Harbi, T.; Mahmoud, W.E. Synthesis and characterization of thin shell hollow sphere NiO nanopowder via ultrasonic technique. *Materials Letters* **2012**, *86*, 28-30.

[21] Xie, D.; Yuan, W.; Dong, Z.; Su, Q.; Zhang, J.; Du, G. Facile synthesis of porous NiO hollow microspheres and its electrochemical lithium-storage performance. *Electrochimica Acta* **2013**, *92*, 87-92.

[22] Liu, L.; Guo, Y.; Wang, Y.; Yang, X.; Wang, S.; Guo, H. Hollow NiO nanotubes synthesized by bio-templates as the high performance anode materials of lithium-ion batteries. *Electrochimica Acta* **2013**, *114*, 42-47.

[23] Yang, Z.; Xu, F.; Zhang, W.; Mei, Z.; Pei, B.; Zhu, X. Controllable preparation of multishelled NiO hollow nanospheres via layer-by-layer self-assembly for supercapacitor application. *Journal of Power Sources* **2014**, *246*, 24-31.

[24] Feng, F.; Zhao, S.; Liu, R.; Yang, Z.; Shen, Q. NiO Flowerlike porous hollow nanostructures with an enhanced interfacial storage capability for battery-to-pseudocapacitor transition. *Electrochimica Acta* **2016**, *222*, 1160-1168.

[25] Hao, S.; Zhang, B.; Ball, S.; Hu, B.; Wu, J.; Huang, Y. Porous and hollow NiO microspheres for high

ACCEPTED MANUSCRIPT

capacity and long-life anode materials of Li-ion batteries. *Materials & Design* **2016**, *92*, 160-165.

[26] Wu, M.K.; Chen, C.; Zhou, J.J.; Yi, F.Y.; Tao, K.; Han, L. MOF–derived hollow double–shelled NiO nanospheres for high–performance supercapacitors. *Journal of Alloys and Compounds* **2018**, *734*, 1-8.

[27] Wang, S.; Li, W.; Xin, L.; Wu, M.; Sun, W.; Lou, X. Pollen-inspired synthesis of porous and hollow NiO elliptical microstructures assembled from nanosheets for high-performance electrochemical energy storage. *Chemical Engineering Journal* **2017**, *321*, 546-553.

[28] Zhu, L.P.; Liao, G.H.; Yang, Y.; Xiao, H.M.; Wang, J.F.; Fu, S.Y. Self-Assembled 3D Flower-Like Hierarchical beta-$Ni(OH)_2$ Hollow Architectures and their In Situ Thermal Conversion to NiO. *Nanoscale Res Lett* **2009**, *4*, 550-557.

[29] Kuang, C.; Zeng, W.; Ye, H.; Li, Y. A novel approach for fabricating NiO hollow spheres for gas sensors. *Physica E: Low-dimensional Systems and Nanostructures* **2018**, *97*, 314-316.

[30] Debao, W.; Caixia, S.; Zhengshui, H.; Fu, X. Fabrication of Hollow Spheres and Thin Films of Nickel Hydroxide and Nickel Oxide with Hierarchical Structures. *J. Phys. Chem. B* **2005**, 1125-1129.

[31] Deng, C.; Hu, H.; Ge, X.; Han, C.; Zhao, D.; Shao, G. One-pot sonochemical fabrication of hierarchical hollow CuO submicrospheres. *Ultrasonics Sonochemistry* **2011**, *18*, 932-937.

[32] Deng, C.; Ge, X.; Hu, H.; Yao, L.; Han, C.; Zhao, D. Template-free and green sonochemical synthesis of hierarchically structured CuS hollow microspheres displaying excellent Fenton-like catalytic activities. *CrystEngComm* **2014**, *16*, 2738-2745.

[33] Ge, X.; Hu, H.; Deng, C.; Zheng, Q.; Wang, M.; Chen, G. Facile sonochemical synthesis of hierarchical $Cu_2O$ hollow submicrospheres with high adsorption capacity for methyl orange. *Materials Letters* **2015**, *141*, 214-216.

[34] Deng, C.; Hu, H.; Shao, G.; Han, C. Facile template-free sonochemical fabrication of hollow ZnO spherical structures. *Materials Letters* **2010**, *64*, 852-855.

[35] Hu, H.; Wang, J.; Deng, C.; Niu, C.; Le, H. Microwave-assisted controllable synthesis of hierarchical CuS nanospheres displaying fast and efficient photocatalytic activities. *Journal of Materials Science* **2018**,

[36] Wang, J.; Xiao, L.; Wen, S.; Chen, N.; Dai, Z.; Deng, J.; Nie, L.; Min, J. Hierarchically porous $SiO_2$/C hollow microspheres: a highly efficient adsorbent for Congo Red removal. *RSC Advances* **2018**, *8*, 19852-19860.

[37] Lei, C.; Pi, M.; Cheng, B.; Jiang, C.; Qin, J. Fabrication of hierarchical porous ZnO/NiO hollow

ACCEPTED MANUSCRIPT

microspheres for adsorptive removal of Congo red. *Applied Surface Science* **2018**, *435*, 1002-1010.

[38] Hu, H.; Chen, G.; Deng, C.; Qian, Y.; Wang, M.; Zheng, Q. Green microwave-assisted synthesis of hierarchical NiO architectures displaying a fast and high adsorption behavior for Congo red. *Materials Letters* **2016**, *170*, 139-141.

[39] Hu, H.; Wang, M.; Xuan, H.; Zhang, K.; Xu, J. Single-crystalline porous NiO nanobiscuits with prompt adsorption activity for Congo red. *Micro & Nano Letters* **2017**, *12*, 987-990.

[40] Xia, X.; Tu, J.; Zhang, Y.; Wang, X.; Gu, C.; Zhao, X.; Fan, H. High-Quality Metal Oxide Core/Shell Nanowire Arrays on Conductive Substrates for Electrochemical Energy Storage. *ACS nano* **2012**, *6*, 5531-5538.

[41] Duan, G.; Cai, W.; Luo, Y.; Sun, F. A Hierarchically Structured $Ni(OH)_2$ Monolayer Hollow‐Sphere Array and Its Tunable Optical Properties over a Large Region. *Advanced Functional Materials* **2010**, *17*, 644-650.

[42] Yan, X.; Tong, X.; Wang, J.; Gong, C.; Zhang, M.; Liang, L. Rational synthesis of hierarchically porous NiO hollow spheres and their supercapacitor application. *Materials Letters* **2013**, *95*, 1-4.

[43] Sing, K.S.W.; Everett, D.H.; Haul, R.A.W.; Moscou, L.; Pierotti, R.A.; Rouquerol, J.; Siemieniewska, T. Reporting Physisorption Data for Gas/Solid Systems with Special Reference to the Determination of Surface Area and Porosity. *Pure and Applied Chemistry* **1985**, *57*, 603-619.

[44] Song, Z.; Chen, L.; Hu, J.; Richards, R. NiO(111) nanosheets as efficient and recyclable adsorbents for dye pollutant removal from wastewater. *Nanotechnology* **2009**, *20*, 275707.

[45] Cheng, B.; Le, Y.; Cai, W.; Yu, J. Synthesis of hierarchical $Ni(OH)_2$ and NiO nanosheets and their adsorption kinetics and isotherms to Congo red in water. *Journal of hazardous materials* **2010**, *185*, 889-897.

[46] Zhao, J.; Tan, Y.; Su, K.; Zhao, J.; Yang, C.; Sang, L.; Lu, H.; Chen, J. A facile homogeneous precipitation synthesis of NiO nanosheets and their applications in water treatment. *Applied Surface Science* **2015**, *337*, 111-117.

[47] Ai, L.; Zeng, Y. Hierarchical porous NiO architectures as highly recyclable adsorbents for effective removal of organic dye from aqueous solution. *Applied Surface Science* **2013**, *s 215-216*, 269-278.

[48] Zheng, Y.; Zhu, B.; Chen, H.; You, W.; Jiang, C. Yu, J. Hierarchical flower-like nickel(II) oxide microspheres with high adsorption capacity of Congo red in water. J Colloid Interface Sci **2017**, 504, 688-696.

ACCEPTED MANUSCRIPT

[49] Rong, X.; Qiu, F.; Qin, J.; Zhao, H.; Yan, J. Yang, D. A facile hydrothermal synthesis, adsorption kinetics and isotherms to Congo Red azo-dye from aqueous solution of NiO/graphene nanosheets adsorbent. Journal of Industrial and Engineering Chemistry **2015**, 26, 354-363.

[50] Ghorai, S.; Sarkar, A.; Raoufi, M.; Panda, A.B.; Schönherr, H.; Pal, S. Enhanced Removal of Methylene Blue and Methyl Violet Dyes from Aqueous Solution Using a Nanocomposite of Hydrolyzed Polyacrylamide Grafted Xanthan Gum and Incorporated Nanosilica. *ACS Applied Materials & Interfaces* **2014**, *6*, 4766-4777.

[51] Zheng, Y.; Wang H.; Cheng B.; You W.; Yu J. Fabrication of hierarchical bristle-grass-like $NH_4Al(OH)_2CO_3$@$Ni(OH)_2$ core-shell structure and its enhanced Congo red adsorption performance. *Journal of Alloys and Compounds* **2018**, 750, 644-654.

ACCEPTED MANUSCRIPT

Published in ***Journal of Porous Materials,*** DOI: 10.1007/s10934-019-00758-2.

Graphical abstract


ACCEPTED MANUSCRIPT

## Highlights

1. The hierarchically porous NiO hollow architectures (HPHAs) were fabricated via a one-pot facile BCD method followed by an annealing process.
2. NiO HPHAs have unusual three-ordered porous features which are beneficial for the adsorption performance towards Congo red in water.
3. The high adsorption capacity contributed to the large specific surface area, the synergistic effect of hierarchically porous structure and the electrostatic attraction.
4. The as-synthesized NiO HPHAs could be promising absorbent as well as catalyst support for the application in water purification and photocatalytic technology.

ACCEPTED MANUSCRIPT

## Figure and table captions

**Fig.1.** Diagram of synthesis of hierarchical β-$Ni(OH)_2$ HSs and NiO HPHAs.

**Fig.2.** XRD patterns of (a) as-prepared precursors and (b) the annealed products.

**Fig. 3.** FESEM and TEM images of as-prepared $Ni(OH)_2$ by CBD method.

**Fig.4.** FESEM (a and b), TEM (c) and HRTEM (d) images, and SAED pattern (e) of as-prepared NiO HPHAs.

**Fig.5.** Plausible schematic illustration of the formation mechanism of NiO HPHA.

**Fig.6.** Nitrogen adsorption/desorption isotherm (a) and pore size distribution curve (b) of as-prepared NiO HPHAs.

**Fig. 7.** (a) The changes of UV-Vis spectra during the removal of CR over NiO HPHAs and (b) Comparison of adsorption capacities for CR with different absorbents.

**Fig. 8.** (a) Changes of adsorption capacities for CR over NiO HPHAs at different initial CR concentrations and (b) pseudo-second-order kinetics for CR adsorption with NiO HPHAs.

**Fig. 9.** (a) Langmuir adsorption isotherm curve and (b) the plot of $C_e/q_e$~$C_e$ for the adsorption of CR onto NiO HPHAs.

**Fig. 10.** Cycling tests for the decolorisation of CR solution.

**Table 1.** Adsorption capacities of CR onto the reported NiO materials.

ACCEPTED MANUSCRIPT